

International Journal of Applied Mathematics in Control Engineering

Journal homepage: <http://www.ijamce.com>

Numerical Control Effect of Electromagnetic Field on the Molten Fluid

Jingcui Liang^a, Wei Wei^{b,*}, Hailong Yang^c, Lianhua Ma^d, Shijun Guo^b^a School of Mathematical and Physical Science and Engineering, Hebei University of Engineering, Handan, Hebei, China^b School of Civil Engineering, Hebei University of Engineering, Handan, Hebei, China^c Handan Purification Equipment Research Institute, Handan, Hebei, China^d College of Quality and Technology Supervision, Hebei University, Baoding, Hebei, China

ARTICLE INFO

Article history:

Received 2 July 2020

Accepted 11 September 2020

Available online 15 September 2020

Keywords:

N-S equation

Electromagnetic fluid

Difference method

Molten metal

Alternating magnetic field

ABSTRACT

Electromagnetic stirring uses an electromagnetic force during the casting process. This enables contact-free modification, control of the electromagnetic formation for liquid metal materials, and improvement of the metallurgical quality of continuous-casting billets. In this paper, the finite difference method is used to discretize the flow-control equation differentially for the numerical simulation of the molten metal material subjected to electromagnetic force. Both velocity and force of the liquid flow in the molten metal material of the billet are analyzed using an electromagnetic field. The continuity difference equation of the electromagnetic fluid motion is derived by discretizing the governing equations of the incompressible electromagnetic fluid mechanics. A staggered grid model is selected to mesh the flow field of the molten metal material for electromagnetic casting, and a flow-difference calculation program is compiled. The numerical calculation is done by the program, and the effect of different excitation-currents and frequencies on the melt-flow is discussed. The results show that the electromagnetic field can control the flow of the molten metal material very well. Different electromagnetic parameters have different effects on the flow of the electromagnetic fluid. Furthermore, there is an optimal moment to suppress the flow of the liquid. Our results confirm that the electromagnetic field can control the formation and solidification process of the molten metal material well, which provides a basis to find realistic casting-process parameters.

Published by Y.X.Union. All rights reserved.

1. Introduction

Recent progress in modern science and technology has quickly increased the requirements of material properties. Electromagnetic stirring, the use of an electromagnetic field and electromagnetic fluid mechanics theory, has attracted the attention of material-science researchers around the world[1-3]. Electromagnetic forming enables electromagnetic braking, electromagnetic heating, electromagnetic stirring, and other processes. The idea is to apply an electromagnetic force during the casting process to achieve contact-free effects, control liquid-metal forming and solidification, and eliminate physical defects such as segregation and hot cracks in ingots. In addition, it can refine grains, improve the solidified structure, and enhance the metallurgical quality of a continuous-casting billet. All of these outcomes would be difficult to achieve by other means. Hence, many scholars are active in this relatively new research field [4-7].

Electromagnetic stirring has many applications, for example,

Vertnik et al[8] used a meshless method to analyze the three-dimensional turbulent molten steel flow and solidification using electromagnetic stirring(EMS). The group also studied the effect of the EMS parameters on the calculated temperature and velocity fields. Yang et al[9] analyzed the magnetic heat-transfer and flow phenomenon during a continuous-casting process using mold electromagnetic stirring. This was done using a 3-D electromagnetic mathematical model and a flow-solidification model. Ren et al[10] developed a 3D mathematical model to simulate the electromagnetic field in a round continuous-casting bloom with electromagnetic stirring (F-EMS). They also investigated the distribution of the electromagnetic force and the effect of current intensity and frequency. An et al. [11] used an electromagnetic torque device to accurately determine the optimum frequency using billet and bloom continuous casting with in-mold electromagnetic stirring. The group also investigated the magnetic characteristics using M-EMS. Trindade et al. [12] studied a fully coupled flow of molten steel, heat transfer, and solidification in a round continuous-casting billet via mold electromagnetic stirring

* Corresponding author.

E-mail addresses: weiwei@hebeu.edu.cn (W. Wei)

(M-EMS). They simulated the electromagnetic stirrer and calculated the Lorenz-force distribution using a finite-element model. Fang et al[13] analyzed the melt flow, level fluctuation, temperature field, and solidification properties during electromagnetic stirring in the continuous-casting mold region of a steel bloom using ANSYS FLUENT. Zhang et al[14] suggested experimental investigations of the impact of a pulsed electric-current and a travelling magnetic-field on the solidification of unalloyed aluminum for different purity-grades via electromagnetic melt stirring. Wang et al[15] performed a coupled three-dimensional numerical simulation of the electromagnetic field and flow field with mold electromagnetic stirrers to study the effects of current, frequency, and the nozzle insertion depth on the flow field. Poole et al[16] developed a model to predict solidification and solute segregation of binary alloys during electromagnetic stirring. They also investigated the effect of final grain size and frequency on segregation. Song et al[17] used a three-dimensional unsteady coupled mathematical model to show that EMS can effectively suppress the central shrinkage cavity as well as center C segregation. Yu and Li[18] investigated the effect of an alternative low-frequency electromagnetic field on ZK60 alloys during the solidification process, which revealed that electromagnetic stirring can facilitate crystallization melting and dendritic crystal breaking. Liu et al[19] found that the distribution of magnetic flux density and electromagnetic force magnitude are nonuniform in a three-dimensional EMS configuration using a low-frequency in-mold rotary electromagnetic-stirrer. Xiong et al[20] showed that electromagnetic stirring can refine the microstructure substantially, which leads to oxides and impurities being melted or broken away from the surface. Chen et al[21] developed a two-dimensional computational model that couples macroscopic heat and fluid flow to show the dynamic evolution of transport phenomena during electromagnetic stirring. They investigated the effect of both intensity and frequency of the current on the magnetic induction intensity by simulating the electromagnetic fields and flow fields using ANSYS software [22-23]. Yoshikawa and Morita [24] used the alternating electromagnetic field generated in an induction furnace to segregate the primary silicon in a hypereutectic Al-Si alloy to yield higher-purity silicon. Oh et al[25] investigated the microstructure and cooling curves of molten alloy in billets, which were fabricated with different electromagnetic stirring parameters. They determined both the formation time and stirring time needed to produce the optimum structure. Li et al[26] applied a strong magnetic field to refine eutectic spacing and find the cause for eutectic degradation. They made the Bi-Mn rod coarser, the rod spacing larger, during the directional solidification of Al-Cu eutectic alloy and the slab-shaped Bi-Mn eutectic alloy, respectively[27].

All of the above studies use electromagnetic stirring. In addition, the metal melt motion in an electromagnetic field is an important research subject. Both distribution and variation of the melt velocity field have important research implications, and the theoretical solution to this question is difficult to find. In addition, no published studies exist, to the best of our knowledge, to analyze the flow phenomena in electromagnetic stirring using the difference equations of electromagnetic fluid mechanics.

In this paper, a mathematical model for the melt flow in a billet with a DC current is developed for the metal melt that interacts with both a time-varying electromagnetic field and the gravitational field. Using the known initial velocity-field, the difference-calculation method was used to analyze the velocity variation of the flow field

for the metal melt controlled by the electromagnetic field. This approach produced some valuable information about the combined effect of an electromagnetic field and a gravitational field on the control of metal-melt flow.

2. Basic equations

Using the incompressible-fluid continuity equation of fluid mechanics, and the N-S equation of an incompressible fluid with intrinsic viscosity, in conjunction with the Ohm equation and the Lorenz-force formula of electromagnetic theory, the governing equation for the two-dimensional incompressible electromagnetic fluid, treated using the artificial compressible method [28-29], can be expressed as

$$\left. \begin{aligned} \frac{\partial u}{\partial t} + a(u,v) + \frac{1}{\rho} \frac{\partial p}{\partial x} - F_{bx} &= \nu \left(\frac{\partial^2 u}{\partial x^2} + \frac{\partial^2 u}{\partial y^2} \right) \\ \frac{\partial v}{\partial t} + b(u,v) + \frac{1}{\rho} \frac{\partial p}{\partial y} - F_{by} &= \nu \left(\frac{\partial^2 v}{\partial x^2} + \frac{\partial^2 v}{\partial y^2} \right) \\ \frac{\partial p}{\partial t} + c^2 \left(\frac{\partial u}{\partial x} + \frac{\partial v}{\partial y} \right) &= 0 \end{aligned} \right\} \quad (1)$$

Here, $a(u,v), b(u,v)$ are the convection terms; ν is the kinematic viscosity; u, v are flow velocity components; ρ is the fluid density; p is the pressure; F_{bx}, F_{by} are volumetric force components per unit volume fluid; c^2 is a free parameter that can be determined by the stable convergence condition of the difference equation.

The convective terms of the non-conservative form can be expressed as

$$\left. \begin{aligned} a(u,v) &= u \frac{\partial u}{\partial x} + v \frac{\partial u}{\partial y} \\ b(u,v) &= u \frac{\partial v}{\partial x} + v \frac{\partial v}{\partial y} \end{aligned} \right\} \quad (2)$$

Using the staggered-grid technique[30-31], in connection with the finite difference method, Eq. (1) can be discretized into the following form:

$$\frac{1}{\Delta t} \left(u_{i+\frac{1}{2},j}^{n+1} - u_{i+\frac{1}{2},j}^n \right) + a_{i+\frac{1}{2},j}^n + \frac{p_{i+1,j}^n - p_{i,j}^n}{\rho \Delta x} - F_{bx} = \nu \left(\frac{u_{i+\frac{3}{2},j}^n - 2u_{i+\frac{1}{2},j}^n + u_{i-\frac{1}{2},j}^n}{\Delta x^2} + \frac{u_{i+\frac{1}{2},j+1}^n - 2u_{i+\frac{1}{2},j}^n + u_{i+\frac{1}{2},j-1}^n}{\Delta y^2} \right) \quad (3)$$

$$\frac{1}{\Delta t} \left(v_{i,j+\frac{1}{2}}^{n+1} - v_{i,j+\frac{1}{2}}^n \right) + b_{i,j+\frac{1}{2}}^n + \frac{p_{i,j+1}^n - p_{i,j}^n}{\rho \Delta y} - F_{by} = \nu \left(\frac{v_{i+1,j+\frac{1}{2}}^n - 2v_{i,j+\frac{1}{2}}^n + v_{i-1,j+\frac{1}{2}}^n}{\Delta x^2} + \frac{v_{i,j+\frac{3}{2}}^n - 2v_{i,j+\frac{1}{2}}^n + v_{i,j-\frac{1}{2}}^n}{\Delta y^2} \right) \quad (4)$$

$$\frac{p_{i,j}^{n+1} - p_{i,j}^n}{\Delta t} + c^2 \left(\frac{u_{i+\frac{1}{2},j}^{n+1} - u_{i-\frac{1}{2},j}^{n+1}}{\Delta x} + \frac{v_{i,j+\frac{1}{2}}^{n+1} - v_{i,j-\frac{1}{2}}^{n+1}}{\Delta y} \right) = 0 \quad (5)$$

It should be noted that the volume force term F_{bx}, F_{by} only

represents electromagnetic forces. The vector formula is $\mathbf{F} = \mathbf{I}_1 \times \mathbf{B}$, where \mathbf{I}_1 is the current-density introduced into the melt, and \mathbf{B} is the magnetic induction intensity acting on the melt.

The non-conservative difference formulas for the convection term are

$$\left. \begin{aligned} a_{i+\frac{1}{2},j}^n &= u_{i+\frac{1}{2},j}^n \frac{u_{i+\frac{3}{2},j}^n - u_{i-\frac{1}{2},j}^n}{2\Delta x} + v_{i+\frac{1}{2},j}^n \frac{u_{i+\frac{1}{2},j+1}^n - u_{i+\frac{1}{2},j-1}^n}{2\Delta y} \\ b_{i,j+\frac{1}{2}}^n &= v_{i,j+\frac{1}{2}}^n \frac{v_{i,j+\frac{3}{2}}^n - v_{i,j-\frac{1}{2}}^n}{2\Delta y} + \hat{u}_{i,j+\frac{1}{2}}^n \frac{v_{i+1,j+\frac{1}{2}}^n - v_{i-1,j+\frac{1}{2}}^n}{2\Delta x} \\ \hat{v}_{i+\frac{1}{2},j}^n &= \frac{1}{4} \left(v_{i,j+\frac{1}{2}}^n + v_{i,j-\frac{1}{2}}^n + v_{i+1,j+\frac{1}{2}}^n + v_{i+1,j-\frac{1}{2}}^n \right) \\ \hat{u}_{i,j+\frac{1}{2}}^n &= \frac{1}{4} \left(u_{i+\frac{1}{2},j}^n + u_{i+\frac{1}{2},j+1}^n + u_{i-\frac{1}{2},j}^n + u_{i-\frac{1}{2},j+1}^n \right) \end{aligned} \right\} (6)$$

3. Calculation model and parameter determination

In this model, based on the stable convergence condition of the difference equation, using the staggered-grid method, Eq. (1) can be expressed as follows:

$$\begin{aligned} u_{i+\frac{1}{2},j}^{n+1} &= \Delta t \cdot v \left(\frac{u_{i+\frac{3}{2},j}^n - 2u_{i+\frac{1}{2},j}^n + u_{i-\frac{1}{2},j}^n}{\Delta x^2} \right. \\ &\quad \left. + \frac{u_{i+\frac{1}{2},j+1}^n - 2u_{i+\frac{1}{2},j}^n + u_{i+\frac{1}{2},j-1}^n}{\Delta y^2} \right) \\ &\quad - \Delta t \cdot u_{i+\frac{1}{2},j}^n \frac{u_{i+\frac{3}{2},j}^n - u_{i-\frac{1}{2},j}^n}{2\Delta x} + u_{i+\frac{1}{2},j}^n \\ &\quad - \frac{\Delta t}{8} \left(v_{i,j+\frac{1}{2}}^n + v_{i,j-\frac{1}{2}}^n + v_{i+1,j+\frac{1}{2}}^n + v_{i+1,j-\frac{1}{2}}^n \right) \\ &\quad - \frac{u_{i+\frac{1}{2},j+1}^n - u_{i+\frac{1}{2},j-1}^n}{\Delta y} - \frac{\Delta t (p_{i+1,j}^n - p_{i,j}^n)}{\rho \Delta x} \end{aligned} \quad (7)$$

As shown in Fig. 1, the calculation model is a rectangular billet with a volume of $1.135m \times 1 \times 1.7m$. The application of a DC current I_1 is shown in Fig. 1, and the alternating magnetic field B occurs along the y -axis, generated by the electromagnet coil.

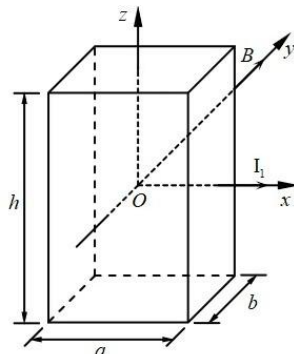


Fig. 1. Schematic of the model.

$$\begin{aligned} v_{i,j+\frac{1}{2}}^{n+1} &= v \Delta t \left(\frac{v_{i+1,j+\frac{1}{2}}^n - 2v_{i,j+\frac{1}{2}}^n + v_{i-1,j+\frac{1}{2}}^n}{\Delta x^2} \right. \\ &\quad \left. + \frac{v_{i,j+\frac{3}{2}}^n - 2v_{i,j+\frac{1}{2}}^n + v_{i,j-\frac{1}{2}}^n}{\Delta y^2} \right) \\ &\quad - v_{i,j+\frac{1}{2}}^n \Delta t \frac{v_{i,j+\frac{3}{2}}^n - v_{i,j-\frac{1}{2}}^n}{2\Delta y} + v_{i,j+\frac{1}{2}}^n \\ &\quad - \frac{\Delta t}{8} \left(u_{i+\frac{1}{2},j}^n + u_{i+\frac{1}{2},j+1}^n + u_{i-\frac{1}{2},j}^n + u_{i-\frac{1}{2},j+1}^n \right) \\ &\quad - \frac{v_{i+1,j+\frac{1}{2}}^n - v_{i-1,j+\frac{1}{2}}^n}{\Delta x} - \frac{\Delta t (p_{i,j+1}^n - p_{i,j}^n)}{\rho \Delta y} \\ &\quad + \Delta t \left(\frac{-\mu W I_1 l_2 \sin(n\omega \Delta t)}{hbl} \times 10^8 \right. \\ &\quad \left. + \rho g ab \left(\delta + \frac{1}{2} \right) \Delta y \right) \quad (\delta = 0,1,2 \dots 8) \end{aligned} \quad (8)$$

$$p_{i,j}^{n+1} = -\Delta t (0.08)^2 \left(\frac{u_{i+\frac{1}{2},j}^{n+1} - u_{i-\frac{1}{2},j}^{n+1}}{\Delta x} + \frac{v_{i,j+\frac{1}{2}}^{n+1} - v_{i,j-\frac{1}{2}}^{n+1}}{\Delta y} \right) + p_{i,j}^n \quad (9)$$

Table 1. Calculation parameters used in the model.

Model parameters	Symbol	Value
Density	ρ	7850kg/m3
Kinematic viscosity	ν	4.81×10^{-7} m2/s
Magnetic permeability	μ	1×10^{-5} H/m
Externally applied current	I_1	1A
Coil current	I_2	20A
Angular velocity	ω	2rad/s
Number of turns of the coil	W	400
Model length	a	1.135m
Model width	b	1m
Model high	h	1.7m
Length of magnetic circuit	l	10m
Time Step	Δt	1s
Step size on the horizontal axis	Δx	0.1135m
Step size on the vertical axis	Δy	0.17m

It is assumed that the steel melt is injected into the square billet from the top surface. As a result, the calculation can be performed in the xz plane. Selecting the time, when the melt is injected into the square billet as the initial moment, the initial velocity distribution in the xz plane is assumed to be represented as shown in Fig. 2[32]. Fig. 3 depicts the difference meshing of the model, and the relevant parameters are shown in Table 1.

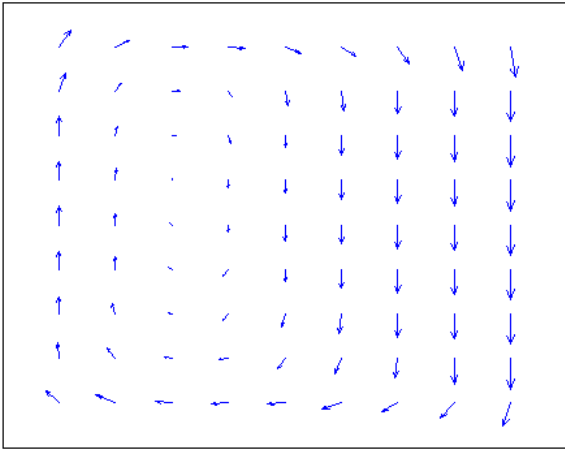


Fig. 2. Schematic map of the initial fluid-velocity field.

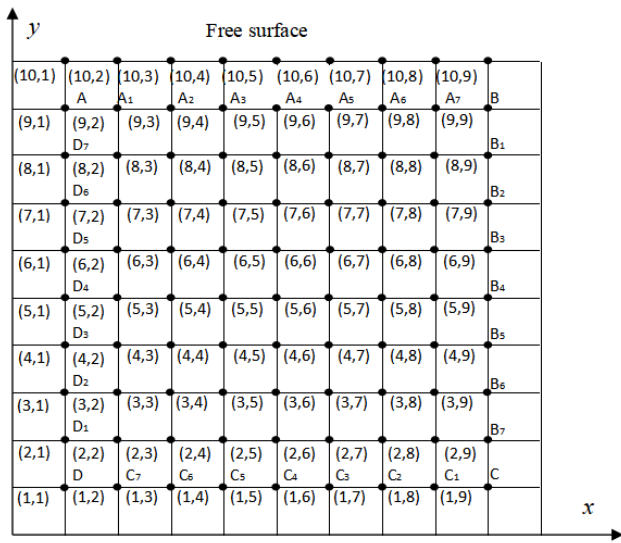


Fig. 3. Sketch map of the difference meshing.

4. Calculation results and analysis

Using the discretized equations, the calculation program was compiled with the computer language C. Taking the unit time as the step size, the effect of the electromagnetic force on the motion of the conductive melt in the square billet can be analyzed using the initial velocity-field.

4.1 Effect of the electromagnetic field on the flow velocity of the conductive melt

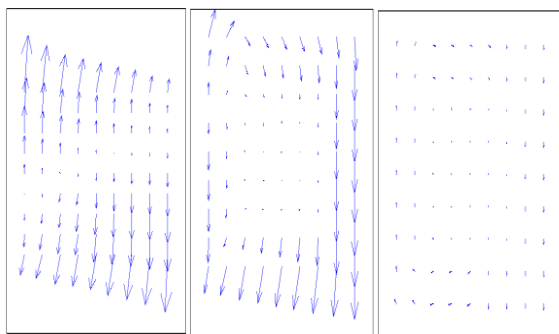
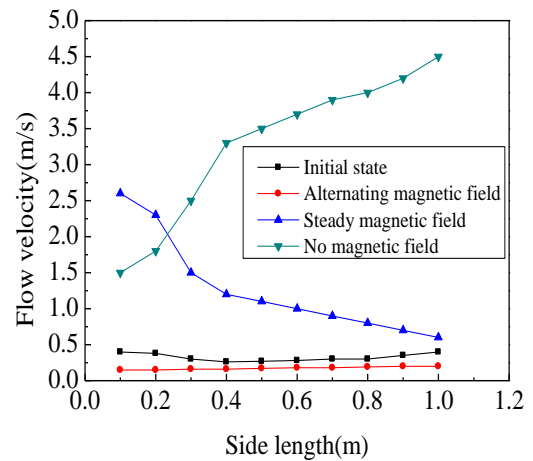


Fig. 4. Velocity field under an alternating magnetic field for different times.

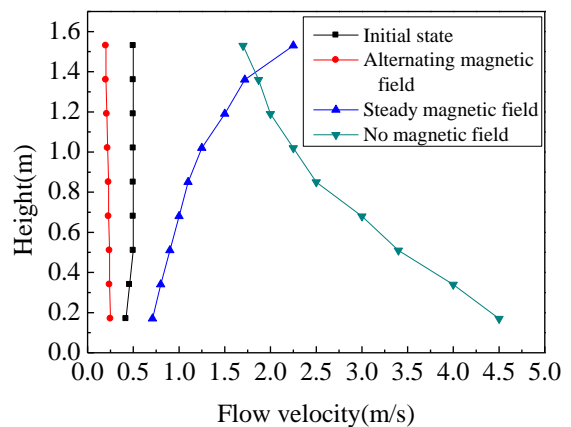
Fig. 4(a)-(c) show the velocity distribution of the flow field for three typical points in time, when the conductive melt was subjected to an alternating magnetic field at a temperature of 700°C. After running the program, it becomes clear that the velocity of each point is greatly reduced at t=23s – more than at the initial time.

The calculated data indicate that the flow direction and velocity of the conductive melt have significant time-varying properties. At t=1-23s, the velocity of the point gradually decreases from the central portion to the outside. The velocity of each point at t=23s is less than for t=0s, while the melt flow in the whole square billet tends to be static. This indicates that the electromagnetic field can significantly inhibit the flow of the conductive melt. As the calculation continues, it is found that the flow of the melt in the square billet changes gradually with time, which results in a new change process. It also shows that t=23s is an optimum time to suppress the liquid flow in this example. At this time, the velocity of each point of the outermost liquid flow is greater than of the inner point, and the velocity near the center of the flow field is smallest.

4.2 Comparison of flow for different magnetic fields



(a) DC side



(b) CB side

Fig. 5. Velocity comparison with three different magnetic fields (T=700°C, t=23s).

To investigate the effect of different magnetic fields on the melt flow in the square billet, the DC and CB sides were chosen as research targets. Fig. 5 shows the velocity analysis of the DC and

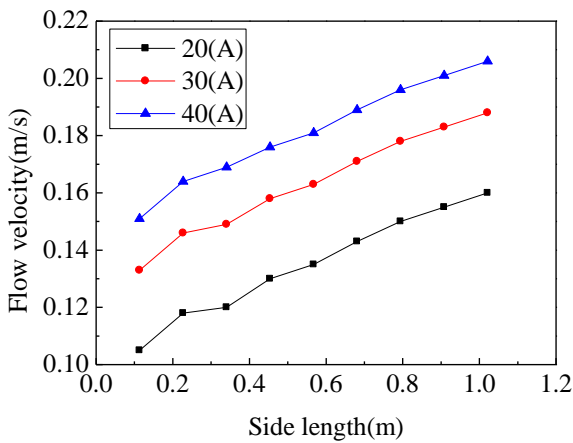
CB sides at $t=23s$ for three different magnetic fields and a conductive melt with a temperature of $700^{\circ}C$. The calculation was carried out under three different conditions: alternating magnetic field, steady magnetic field, and no magnetic field, which correspond to curves 2, 3, and 4, respectively. Curve 1 is the initial state at $t=0s$.

The velocity of the point is the smallest under the alternating electromagnetic field. This means that the velocity of the liquid flow can be reduced in a short time, and the effect of suppressing the liquid flow is optimized. When a steady magnetic field and no magnetic field were applied, there was no effect on the inhibition of liquid flow, and the velocity of the corresponding point was greater than for the alternating magnetic field.

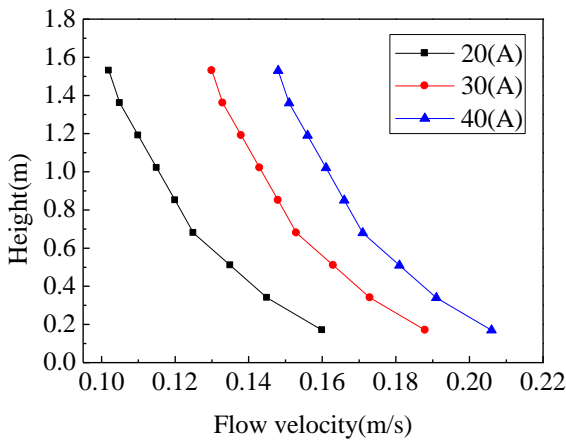
4.3 Effect of excitation current and frequency on the flow velocity

We found that the effect of the electromagnetic field on the melt in the outer region is stronger than for in the inner region. Therefore, the two paths DC and CB were selected to discuss the effect of the excitation current on the flow velocity.

The velocity curves of the DC and CB sides, with different excitation currents, are shown in Fig. 6. The curves 1, 2, and 3 denote $I_2=20A$, $30A$, and $40A$, respectively. Furthermore, the origin of the coordinates is located at the lower left corner of the billet.



(a) DC side



(b) CB side

Fig. 6. Velocity comparison for the DC and CB sides($t=23s$).

When the excitation current increases gradually by 20A, 30A,

and 40A, the velocity of the point at the DC and CB sides also increases uniformly. In other words, as the excitation current increases, the Lorentz force of the melt increases too. This means, the flow velocity of the conductive melt is proportional to the excitation current, and the direction of flow can be determined by adjusting the action of the electromagnetic force.

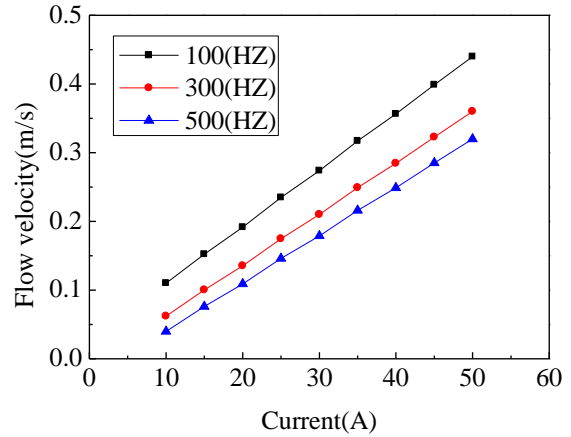
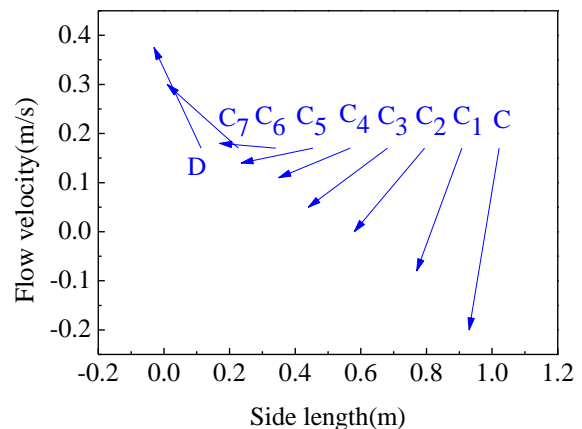


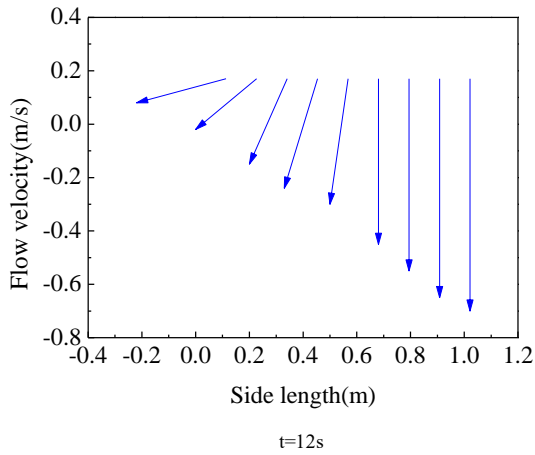
Fig. 7. Effect of different frequencies and currents on the flow velocity at point B($t=23s$).

Fig.7 shows the effect of different currents on the flow velocity at point B at $t=23s$, for different frequencies. It can be seen that, for the same frequency, as the current I_2 in the coil of the electromagnet increases, the velocity at B point also increases continuously. When the frequency increases gradually for the same current, the velocity of the point decreases continuously. Upon increasing the same frequency, the decreasing magnitude of the flow velocity becomes smaller. In addition, when the current is small, the velocity reduction is relatively small. As the current increases, the velocity reduction increases, which is in good agreement with published results[32]. In summary, when the frequency and current increase simultaneously, the flow velocity of the outermost liquid flow in the melt decreases gradually. However, the magnitude of the change is not constant.

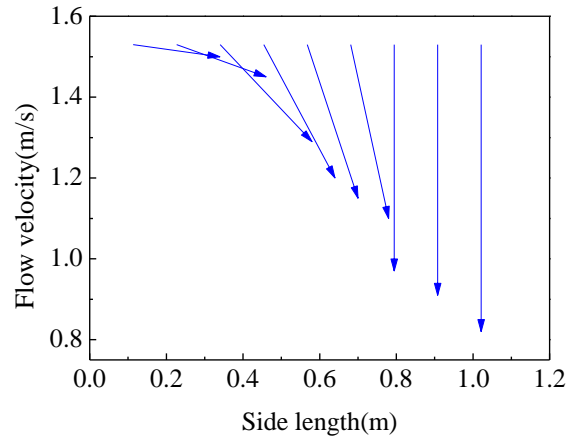
4.4 Analysis of the relationship between electromagnetic force and flow



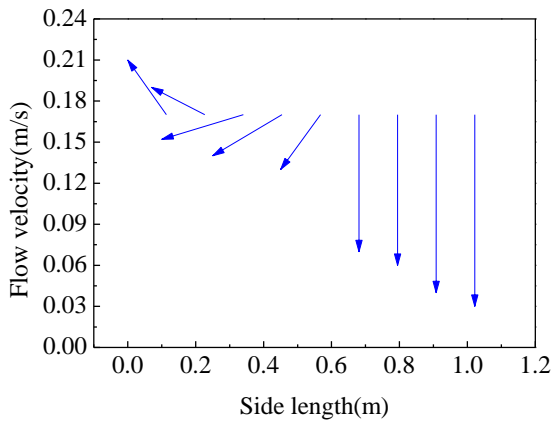
(a) $t=0s$



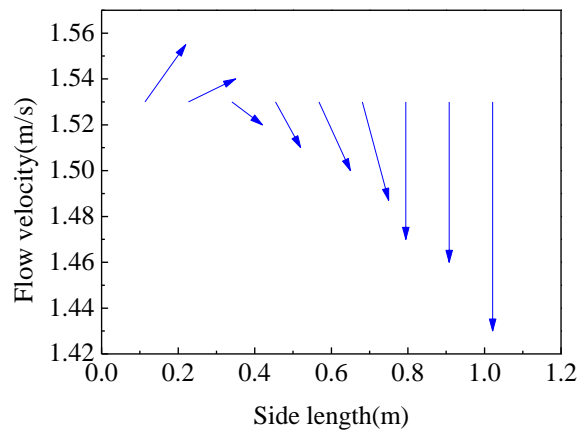
t=12s



(b) t=12s



(c) t=23s



(c) t=23s

Fig. 8. Flow velocity analysis on the DC side(t=0,12,23s).

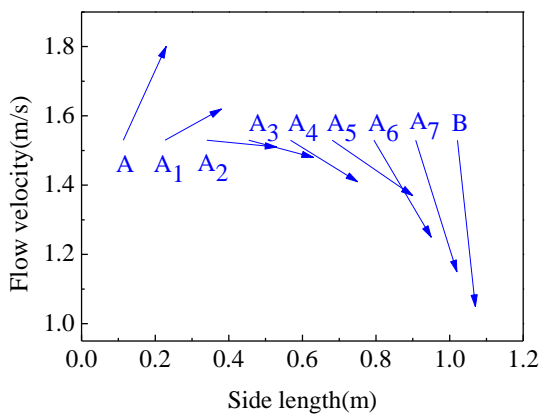
Fig. 8(a) shows the velocity of the liquid on the DC side at t=0s. Due to its initial downward direction, the velocity of the points C, C₁, ..., C₆, who are subjected to a downward net force, must increase significantly at t=12s - see Fig. 8(b). In addition, because of its initial upward direction and downward net force, from t=0s to t=12s, the velocity of points C₇ and D changes to downward at t=12s. For t=13-23s, the velocity of the points C, C₁, ..., C₆ must be reduced continuously due to the upward net force, compared to t=12s. At this time, the velocity of points C₇ and D also decreases, which represents the final scene - see t=23s in Fig. 8(c).

Fig. 9. Flow velocity analysis for the AB side(t=0,12,23s).

Fig. 9(a) shows the velocity of the liquid on AB side at t = 0s. Due to its initial upward direction, the velocity of the points A, A₁, which are subjected to a downward net-force, must decrease, and the direction changes to downward for t=12s - see Fig. 9(b). Because of its initial downward directions, the velocity of points A₂, A₃, ..., B must be increased continuously, and subject to a downward net-force. In the period of t=13-23s, due to the upward net-force, the movement of the points A, A₁ becomes upward again. However, the value is smaller than the corresponding value at t=0s in Fig. 9(c). Simultaneously, the velocity of the points A₂, A₃, ..., B with the downward velocity must be continuously reduced, when subjected to the upward net-force.

In summary, considering the two cases in Fig. 8 and Fig. 9, and a period t=1-23s, because the points on the DC or AB sides are subjected to two different net forces in different directions, the velocity is reduced compared to the initial time. This effectively suppresses the liquid flow. After verification, similar results can be obtained by analyzing the flow velocity for other sides.

The calculation results reveal that the direction of the electromagnetic force of the melt in the billet changes, up and down, due to the pulsating characteristics of the alternating electromagnetic field. In addition, the force of the melt in different liquid layers is also different. As the liquid layer decreases, the pressure of the liquid flow increases, which indicates that the size of the net force inside the melt also changes. When the direction of



(a) t=0s

the electromagnetic force is downward, and the pressure is downward too, the direction of the net force is downward. This facilitates the melt flow. When the direction of the electromagnetic force is upward and combined with the downward pressure, the forces act on each other, which inhibit the melt flow.

5. Conclusions

In this paper, a metal-melt flow-field with a DC current was used to numerically study the effect of different electromagnetic parameters on the melt in an electromagnetic field using the N-S equation for electromagnetic fluid motion, which was discretized via the finite difference method. The calculated results reveal that the alternating-current magnetic field can suppress the liquid-flow when the conductive molten metal is subjected to the alternating magnetic-field, the steady magnetic-field, and the non-magnetic-field. The velocity of each point in the flow field is smaller than at the beginning.

Therefore, a careful selection of the electromagnetic parameters and time history can control the flow of the conductive metal-melt that is injected into the square billet. This enables some control of the metal-solidification process and morphology. In addition, electromagnetic parameters, metal parameters, initial velocity, temperature, and history can have a significant effect on the motion of the melt. Therefore, when applying this technology under specific working conditions, a detailed analysis and calculation should be performed that takes into account the actual conditions. Given the different control requirements such as melt flow rate, flow direction, and area, the electromagnetic force can be used to control the molding and solidification process, improve the quality and defects of the slab. Our results provide a good approach to determine suitable casting parameters.

Acknowledgements

This work was supported by the National Natural Science Foundation of China (Grant No. 11572109), and Science and Technology Development Programs of Handan City (Grant No. 1721211051-4; Grant No.19422111008-23).

References

- [1] Lu B W, Cui X F, Jiang L P, et al. Influence of electromagnetic stirring on microstructure and wear resistance of plasma arc deposited shape memory alloy[J]. *Surface and Coatings Technology*, 2019, 359:125-131.
- [2] Li Y, Deng A Y, Li H, et al. Numerical study on flow, temperature, and concentration distribution features of combined gas and bottom-electromagnetic stirring in a ladle[J]. *Metals*, 2018, 8(1): 76.
- [3] Waryoba D R and Roberts W. Application of electromagnetic processing for development of high-performance sintered powder metal parts[J]. *Current Applied Physics*, 2017,17(10): 1288-1297.
- [4] Hu D, Yan Y and Xu X, et al. Energy saving optimal design and control of electromagnetic brake on passenger car[J]. *Mechanical Sciences*, 2019, 10(1): 57-70.
- [5] Ran J, Hua F, Yong G W, et al. Analysis and simulation of temperature control for battery pole piece electromagnetic heating roller[J]. *Journal of System Simulation*, 2018, 30(6): 2245-2250.
- [6] Jeng S L, Su D P, Lee J T, et al. Effects of electromagnetic stirring on the cast austenitic stainless steel weldments by gas tungsten arc welding[J]. *Metals*, 2018, 8(8): 630.
- [7] Zeng J, Chen W Q, Yang Y D, et al. A review of permanent magnet stirring during metal solidification. *Metallurgical and materials transactions B*, 2017, 48(6): 3083-3100.
- [8] Vertnik R, Mramor K and Šarler B. Solution of three-dimensional temperature and turbulent velocity field in continuously cast steel billets with electromagnetic stirring by a meshless method[J]. *Engineering Analysis with Boundary Elements*, 2019, 104: 347-363.
- [9] Yang B, Deng A Y, Li Y, et al. Numerical simulation of flow and solidification in continuous casting process with mold electromagnetic stirring[J]. *Journal of Iron and Steel Research International*, 2019, 26(3): 219-229.
- [10] Ren B, Chen D, Xia W, et al. Numerical simulation of electromagnetic field in round bloom continuous casting with final electromagnetic stirring[J]. *Metal*, 2018, 8(11): 903.
- [11] An H, Bao Y, Wang M, et al. Electromagnetic torque detecting for optimization of in-mould electromagnetic stirring in the billet and bloom continuous casting[J]. *Ironmaking & Steelmaking*, 2018, 1-10.
- [12] Trindade L B, Nadalon J E A, Contini A C, et al. Modeling of solidification in continuous casting round billet with mold electromagnetic stirring (M-EMS)[J]. *Steel research international*, 2017,88(4): 1600319.
- [13] Fang Q, Ni H, Zhang H, et al. The effects of a submerged entry nozzle on flow and initial solidification in a continuous casting bloom mold with electromagnetic stirring[J]. *Metals*, 2017, 7(4): 146.
- [14] Zhang Y H, Rübiger D and Eckert S. Solidification of pure aluminium affected by a pulsed electrical field and electromagnetic stirring[J]. *Journal of materials science*, 2016, 51(4): 2153-2159.
- [15] Wang B X, Chen W, Chen Y, et al. Coupled numerical simulation on electromagnetic field and flow field in the round billet mould with electromagnetic stirring[J]. *Ironmaking & Steelmaking*, 2015,42(1): 63-69.
- [16] Poole G M, Heyen M, Nastac L, et al. Numerical modeling of macrosegregation in binary alloys solidifying in the presence of electromagnetic stirring[J]. *Metallurgical and Materials Transactions B*, 2014, 45(5): 1834-1841.
- [17] Song X P, Cheng S S and Cheng Z J. Mathematical modelling of billet casting with secondary cooling zone electromagnetic stirrer[J]. *Ironmaking & Steelmaking*, 2013,40(3):189-198.
- [18] Yu Y D and Li C X. The effect of alternative low frequency electromagnetic field on the solidification microstructure and mechanical properties of ZK60 alloys[J]. *Materials & Design*, 2013, 44: 17-22.
- [19] Liu H, Xu M, Qiu S, et al. Numerical simulation of fluid flow in a round bloom mold with in-mold rotary electromagnetic stirring[J]. *Metallurgical and Materials Transactions B*, 2012, 43(6): 1657-1675.
- [20] Xiong B W, Cai C C, Wan H, et al. Fabrication of high chromium cast iron and medium carbon steel bimetal by liquid-solid casting in electromagnetic induction field[J]. *Materials & Design*, 2011, 32(5): 2978-2982.
- [21] Chen X R, Zhang Z F and Xu J. Effects of annular electromagnetic stirring processing parameters on semi-solid slurry production[J]. *Transactions of Nonferrous Metals Society of China*, 2010, 20: 873-877.
- [22] Chen X R, Zhang Z F, Liang B, et al. Numerical simulation of electromagnetic field and flow field in the course of preparation semi-solid slurry of aluminum alloy[J]. *Foundry Technology*, 2010, 31(4): 482-486.
- [23] Chen X R, Zhang Z F, Xu J, et al. Numerical simulation of electromagnetic field, flow field and temperature field in semi-solid slurry preparation by electromagnetic stirring[J]. *The Chinese Journal of Nonferrous Metals*, 2010, 20(5): 937-945.
- [24] Yoshikawa T and Morita K. Refining of silicon during its solidification from a Si-Al melt[J]. *Journal of Crystal Growth*, 2009, 311(3): 776-779.
- [25] Oh S W, Bae J W and Kang C G. Effect of electromagnetic stirring conditions on grain size characteristic of wrought aluminum for rheo-forging[J]. *Journal of Materials Engineering and Performance*, 2008, 17(1): 57-63.
- [26] Li X, Ren Z and Fautrelle Y. Effect of a high axial magnetic field on the microstructure in a directionally solidified Al-Al₂Cu eutectic alloy[J]. *Acta Materialia*, 2006, 54(20): 5349-5360.
- [27] Li X, Ren Z and Fautrelle Y. Effect of high magnetic fields on the microstructure in directionally solidified Bi-Mn eutectic alloy[J]. *Journal of Crystal Growth*, 2007, 299(1): 41-47.
- [28] Ohwada T and Asinari P. Artificial compressibility method revisited: asymptotic numerical method for incompressible Navier-Stokes equations[J]. *Journal of Computational Physics*, 2010, 229(5): 1698-1723.
- [29] Zhang J K, Dong H, Zhou E Z, et al. A combined method for solving 2D incompressible flow and heat transfer by spectral collocation method and artificial compressibility method[J]. *International Journal of Heat and Mass Transfer*, 2017, 112: 289-299.
- [30] Cecere D and Giacomazzi E. An immersed volume method for large eddy simulation of compressible flows using a staggered-grid approach[J]. *Computer Methods in Applied Mechanics and Engineering*, 2014, 280: 1-27.

- [31] Chen H X, Sun S Y and Zhang T. Energy stability analysis of some fully discrete numerical schemes for incompressible Navier-Stokes equations on staggered grids[J]. Journal of Scientific Computing, 2018, 75(1): 427-456.
- [32] Shekli. Fluid Flow in Metallurgy. 1985, 1st Ed. Beijing, China: The Metallurgical Industry Press(in Chinese).



Jingcui Liang received her MS Degree in Computational Mathematics from Yanshan University, Qinhuangdao, China, in 2005. Her current research interests include computational mathematics and computational electromagnetic fluid mechanics.
Email: liangjingcui@hebeu.edu.cn



Wei Wei received his MS Degree in Solid mechanics from Yanshan University, Qinhuangdao, China, in 2005. He later received the PhD degree in mechanics at Beijing University of technology, Beijing, China, in 2017. His research interest is computational mechanics.
Email: weiwei@hebeu.edu.cn



Hailong Yang received his Bachelor's degree in Chemical Engineering and Technology from Harbin Engineering University, Harbin, China, in 2002. Later he worked at Handan purification equipment research institute.
Email: yhl_hl@163.com



Lianhua Ma received his MS and PhD degree in engineering mechanics from Beijing University of technology, Beijing, China, in 2012. He is currently a associate Professor of College of Quality and Technology Supervision, Hebei University. His current research interest is composite mechanics.
Email: lhma@hbu.edu.cn



Shijun Guo received his MS and PhD degree in Engineering mechanics from Beijing University of technology, Beijing, China, in 2014. His current research interest is composite mechanics.
Email: guoshijun@hebeu.edu.cn